Crustal depth of emplacement of the Early Jurassic Aishihik and Tatchun batholiths, west-central Yukon

***M.J. Topham*[1]**
Department of Earth, Ocean, and Atmospheric Sciences, The University of British Columbia

M.M. Allan*[2]*, J.K. Mortensen, C.J.R. Hart
Mineral Deposit Research Unit, University of British Columbia

M. Colpron, P.J. Sack
Yukon Geological Survey

Topham, M.J., Allan, M.M., Mortensen, J.K., Hart, C.J.R., Colpron, M. and Sack, P.J., 2016. Crustal depth of emplacement of the Early Jurassic Aishihik and Tatchun batholiths, west-central Yukon. *In:* Yukon Exploration and Geology 2015, K.E. MacFarlane and M.G. Nordling (eds.), Yukon Geological Survey, p. 233-251, including appendices.

ABSTRACT

Early Jurassic plutons in west-central Yukon were emplaced during accretion of the Intermontane terranes onto the western North American margin, and their exhumation is recorded in the sedimentological and geochronological record. Here the aluminum-in-hornblende geothermobarometer is applied to the 200-197 Ma Tatchun batholith and the 188-180 Ma Aishihik batholith, to estimate crystallization depths and exhumation rates. The Tatchun batholith crystallized at 6.4-7.2 kbar (23-26 km), whereas the Aishihik batholith was emplaced at 3.4-4.2 kbar (12-15 km). The Tatchun batholith exhumed at a rate of ~1.2-2.0 mm/a after crystallization, and was likely exposed at surface by the Middle Jurassic. Although subvolcanic equivalents of the Tatchun batholith have been lost to erosion, it could be prospective for deformed copper deposits such as Minto and Carmacks Copper. Hypabyssal and water-saturated phases of the Aishihik batholith suggest that portions of the batholith could be at, or just below, an appropriate crustal level for magmatic-hydrothermal mineralization.

[1]*matthewjtopham@gmail.com*

[2]*mallan@eos.ubc.ca*

INTRODUCTION

Late Triassic to Early Jurassic arc-related plutons of the British Columbia, Yukon and eastern Alaska Cordillera record the growth of the metallogenically significant Stikinia and Quesnellia arc terranes, and their accretion to the western North American margin (*e.g.*, Mortensen *et al.*, 2000; Nelson *et al.*, 2013). Current field mapping and geochronological studies have led to the definition of four discrete arc-related plutonic suites in Yukon of this age range (Gordey and Makepeace, 2001; Joyce *et al.*, 2016): the Stikine suite (220-206 Ma), which represents the plutonic roots of the peri-Laurentian Stikinia and Quesnellia arc terranes; the Minto suite (204-195 Ma), which likely represents the onset of arc accretion and continental arc magmatism; and the Long Lake (188-180 Ma) and Bryde suites (178-160 Ma), which record continental arc magmatism associated with the evolving Cordilleran orogeny (Nelson *et al.*, 2013; Fig. 1).

As indicated by regional cooling ages (Breitsprecher and Mortensen, 2004; Joyce *et al.*, 2015) and the Early to Middle Jurassic sedimentological and detrital zircon record (Dickie and Hein, 1995; Hart *et al.*, 1995; Hart, 1997; Lowey, 2004; Colpron *et al.*, 2015), Late Triassic to Early Jurassic batholiths were emplaced into crust that exhumed in the Early to Middle Jurassic to form the fault-bound flanks of the subsiding Whitehorse trough terrestrial to marine basin. The depth and timing of pluton emplacement, the rate of crustal exhumation and the age of sedimentation from igneous source rocks are generally poorly constrained, but are important considerations for tectono-structural reconstructions of the evolving Cordilleran orogeny in the Jurassic. These factors also bear on the likelihood of forming and preserving Late Triassic to Early Jurassic porphyry copper deposits in Yukon.

In this contribution, we build on previous geothermobarometric investigations of Early Jurassic plutons (McCausland *et al.*, 2002; Tafti, 2005) by applying the same empirical aluminum-in-hornblende geothermobarometer to the Aishihik and Tatchun batholiths of west-central Yukon, which represent the Long Lake and Minto plutonic suites, respectively (Fig. 1; Joyce *et al.*, 2016). This pressure-depth information is combined with magmatic ages (Joyce *et al.*, 2016) and cooling ages of the plutons (Joyce *et al.*, 2015) to estimate rates of crustal exhumation and to gauge the likelihood of preserving shallow magmatic-hydrothermal systems.

GEOLOGIC SETTING

The latest Triassic to Jurassic evolution of the Cordilleran hinterland in Yukon is characterized by accretion of the Intermontane terranes (Quesnellia, Slide Mountain terrane, Stikinia, Yukon-Tanana terrane, Cache Creek terrane) to the western North American margin, accompanied by tectonic thickening and continental arc magmatism, and followed by concurrent exhumation and synorogenic basin formation (Whitehorse trough; *e.g.*, Mihalynuk *et al.*, 1994, 2004; Nelson *et al.*, 2013; Colpron *et al.*, 2015). The distribution of upper Triassic volcanic and sedimentary rocks of Stikinia and Quesnellia (Lewes River Group) in southern Yukon tapers northwestward, where northwest of the confluence of the Pelly River and Yukon River, only age-equivalent plutonic rocks of the Stikine suite are exposed (Fig. 1).

Lewes River Group rocks are unconformably overlain by Lower to Middle Jurassic (Hettangian to Bajocian) terrestrial to marine sedimentary rocks of the Laberge Group, which were fed igneous detritus derived from mountainous terrain via river systems into the Whitehorse trough (Fig. 1; Hart *et al.*, 1995; Hart, 1997; Lowey, 2008; Colpron *et al.*, 2015). The Laberge Group is divided into two distinct facies: the Richthofen Formation in the south, which consists of distal deep-marine facies turbidite rocks and mass flow conglomerate rocks, and the Tanglefoot Formation in the north, which is dominated by proximal-facies, shallow-marine to fluvial sandstone and conglomerate, as well as mudstone and minor limestone (Lowey, 2008; Colpron *et al.*, 2015). Interbedded horizons of Nordenskiold tuff, with U-Pb zircon ages between 188 and 186 Ma, occur in both the Tanglefoot and Richthofen formations, and are coeval with, and derived from, Long Lake suite magmatism (Hart, 1997; Fillmore, 2006; Colpron and Friedman, 2008; Joyce *et al.*, 2016). The stratigraphy of the Laberge Group is interpreted to record the exhumation of Late Triassic to Early Jurassic plutons of the Stikine, Minto, Long Lake and Bryde plutonic suites that were emplaced during the Cordilleran orogeny (Hart, 1997; Colpron *et al.*, 2015). Specifically, Late Pliensbachian (183 Ma) and younger conglomerate rocks of the Tanglefoot Formation contain approximately 60 to 80% plutonic clasts derived from the adjacent Late Triassic to Early Jurassic plutons (Dickie and Hein, 1995; Lowey, 2008).

Latest Triassic to Early Jurassic plutonic rocks are exposed as large batholiths outboard and inboard of exposures of the Lewes River Group (Fig. 1). Minto suite plutons include the Granite Mountain batholith and Minto pluton, which

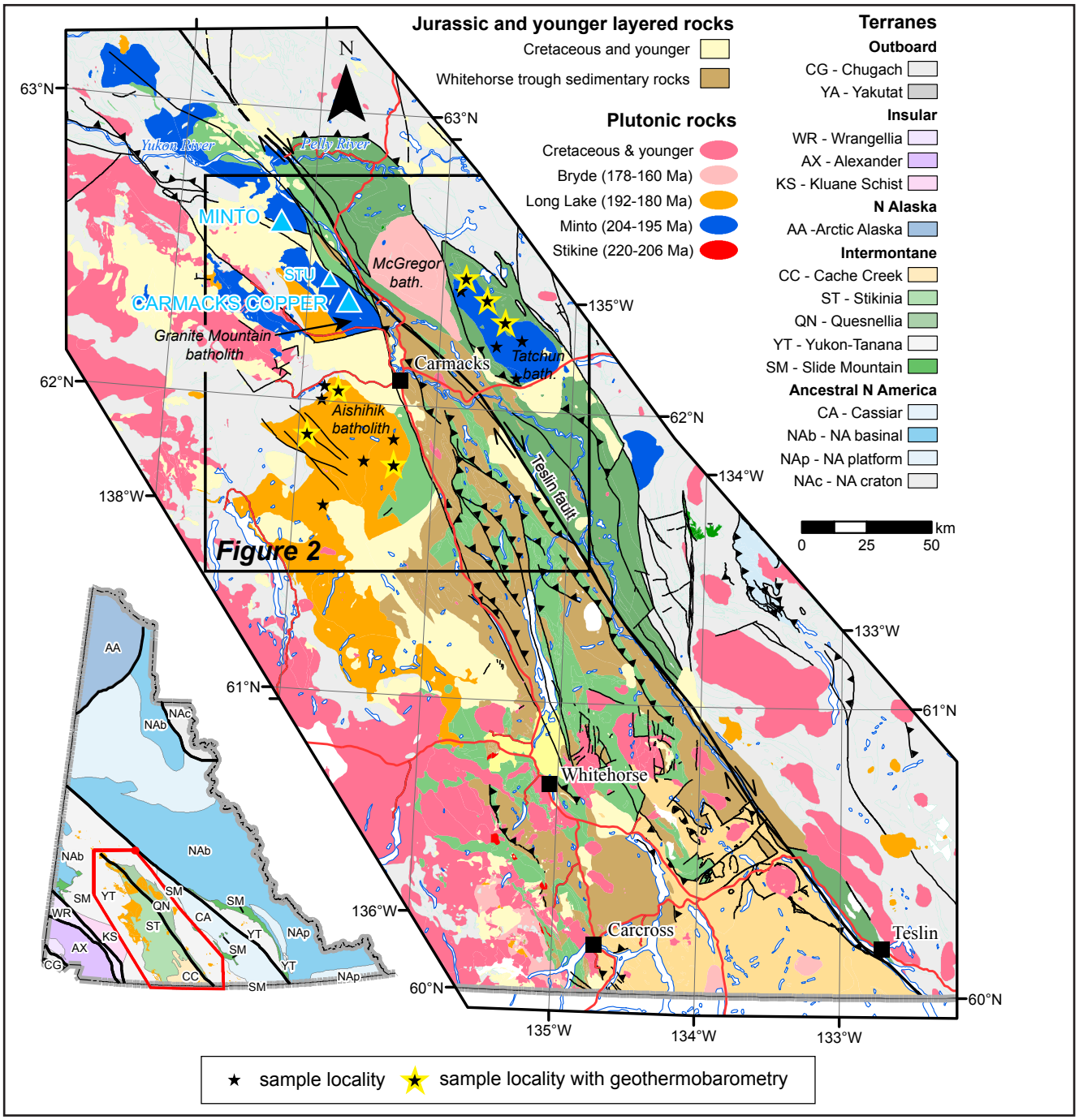

Figure 1. *Simplified regional geologic map of the Whitehorse trough region, highlighting Late Triassic to Early Jurassic plutonic suites. Geological data from Yukon Geological Survey (2015). Sample localities are indicated with the black stars, and samples used for geothermobarometry are highlighted in yellow.*

host the Carmacks Copper and Minto Cu-Au-Ag deposits, respectively. North of the mid-Cretaceous dextral strike-slip Teslin fault system, the Minto suite is represented by the *ca.* 200-197 Ma Tatchun batholith (Fig. 1; Colpron, 2011). The Aishihik batholith, located east of Aishihik Lake and southwest of Carmacks, is composed of 188-180 Ma granitoid rocks of the Long Lake suite (Johnston *et al.*, 1996; Hart, 1997; Joyce *et al.*, 2016). The Minto and Long Lake plutonic suites are compositionally heterogeneous, generally metaluminous, and demonstrate continental arc geochemical signatures (Mortensen *et al.*, 2000; Joyce *et al.*, 2016). Plutons of the Bryde suite include the McGregor

batholith north of Carmacks (Figs. 1 and 2) and several smaller plutons in southern Yukon (Fig. 1), but are not addressed in this study.

The regional tectonic fabric of the study area is a series of west-verging-thrust sheets, in which the Aishihik batholith is interpreted as an east-dipping, foliation-parallel, tabular intrusion (Hart, 1997; Johnston and Canil, 2007; Mira Geoscience, 2014). A weakly to moderately developed magmatic foliation is especially well developed near the margins of the pluton, which is consistent with a syntectonic interpretation (Johnston and Canil, 2007). Similarly, the Tatchun batholith is bound by southwest-verging thrust faults (Buffett *et al.*, 2006). The Tatchun batholith intrudes the Semenof block, which consists of Devonian to Permian volcanic and sedimentary arc rocks of the Boswell assemblage, which forms the basement to Mesozoic arc assemblages of Quesnellia (Semenof Formation; Templeman-Kluit, 1984, 2009; Simard and Devine, 2003; White *et al.*, 2012). Regional geophysical inversion modeling (Mira Geoscience, 2014) confirms previous interpretations by Colpron (2011) that the Tatchun batholith is a subhorizontal body. The tectonic setting of the Tatchun batholith is broadly similar to that suggested for the Aishihik batholith by Johnston and Canil (2007), in that it was emplaced into actively amalgamating lithotectonic domains.

Late Triassic to Early Jurassic plutonic rocks of west-central Yukon were exhumed shortly after their emplacement, as indicated by the preponderance of Early to Middle Jurassic cooling ages of batholiths and their country rocks (Breitsprecher and Mortensen, 2004; Colpron, 2011; Joyce *et al.*, 2015). Likewise, the eventual exposure and erosion of these plutons at surface is marked by the steady supply of igneous-derived detritus throughout the Early to Middle Jurassic sedimentation history of the Laberge Group (Hart *et al.*, 1995; Hart, 1997; Lowey, 2008; Colpron *et al.*, 2015). By the Late Jurassic, magmatic activity waned considerably, and by the end of the Jurassic, both crustal exhumation of plutonic rocks and sedimentation in the Whitehorse trough had ceased (Colpron *et al.*, 2015).

METALLOGENIC SETTING

In British Columbia, Late Triassic to Early Jurassic arc magmatism in Quesnellia and Stikinia has a well-documented connection to porphyry Cu-(Mo-Au) mineralization (*e.g.*, Logan and Mihalynuk, 2014). In Yukon, the plutonic roots of these arcs are exposed as the Stikine and Minto suites. However, possible examples of age-equivalent subvolcanic porphyry Cu-Au mineralization are restricted to a small number of occurrences in southern Yukon (*e.g.*, King Lake, Yukon MINFILE 115D 104 and Red Ridge, Yukon MINFILE 115D 100). In general, plutons of the Stikine and Minto suites were emplaced at mid-crustal pressures, as indicated by previous geothermobarometric studies (*e.g.*, McCausland *et al.*, 2002; Tafti, 2005) and by the presence of magmatic epidote (Tafti, 2005; Johnston *et al.*, 1996), which is indicative of high pressure (Zen and Hammarstrom, 1984). Accordingly, plutons of this age are generally poor targets for coeval, shallow-crustal porphyry, skarn, or epithermal mineralization.

Regardless, the Minto and Carmacks Copper deposits (Figs. 1 and 2) are two significant Yukon examples of intrusion-related Cu-Au-Ag mineralization associated with latest Triassic to Early Jurassic plutons. They are broadly characterized by sulphide mineralization hosted by schistose to gneissic to migmatitic rocks that have subsequently been intruded by massive granodiorite at mid-crustal levels in excess of 20 km (Tafti, 2005; Hood, 2012). These deposits have been variably interpreted as deformed porphyry systems (Mortensen *et al.*, 2000; Tafti and Mortensen, 2004), shear-hosted magmatic-hydrothermal deposits (Hood, 2012), iron-oxide copper gold (Mercer and Sagman, 2012), and sediment-hosted copper deposits (Pearson and Clark, 1979). Although the details of ore genesis at Minto and Carmacks Copper have been controversial, the association of mineralization with deeply emplaced plutonic rocks implies a unique exploration target.

PREVIOUS PRESSURE-DEPTH CONSTRAINTS

Estimations of the crustal depth of magma emplacement require an independent constraint on the pressure of crystallization, such as a pressure-sensitive mineral or mineral assemblage geobarometer. One such geobarometer is based on the empirical correlation between the total Al content of calcic amphibole and its pressure (P) of crystallization (Hammarstrom and Zen, 1986). The Al-in-hornblende geobarometer initially calibrated compositional analyses of hornblende from various Cordilleran plutons with independently constrained crystallization pressures derived from stratigraphic arguments or equilibrium mineral assemblages in contact metamorphic aureoles (Hammarstrom and Zen, 1986; Hollister *et al.*, 1987). The geobarometer was corrected for

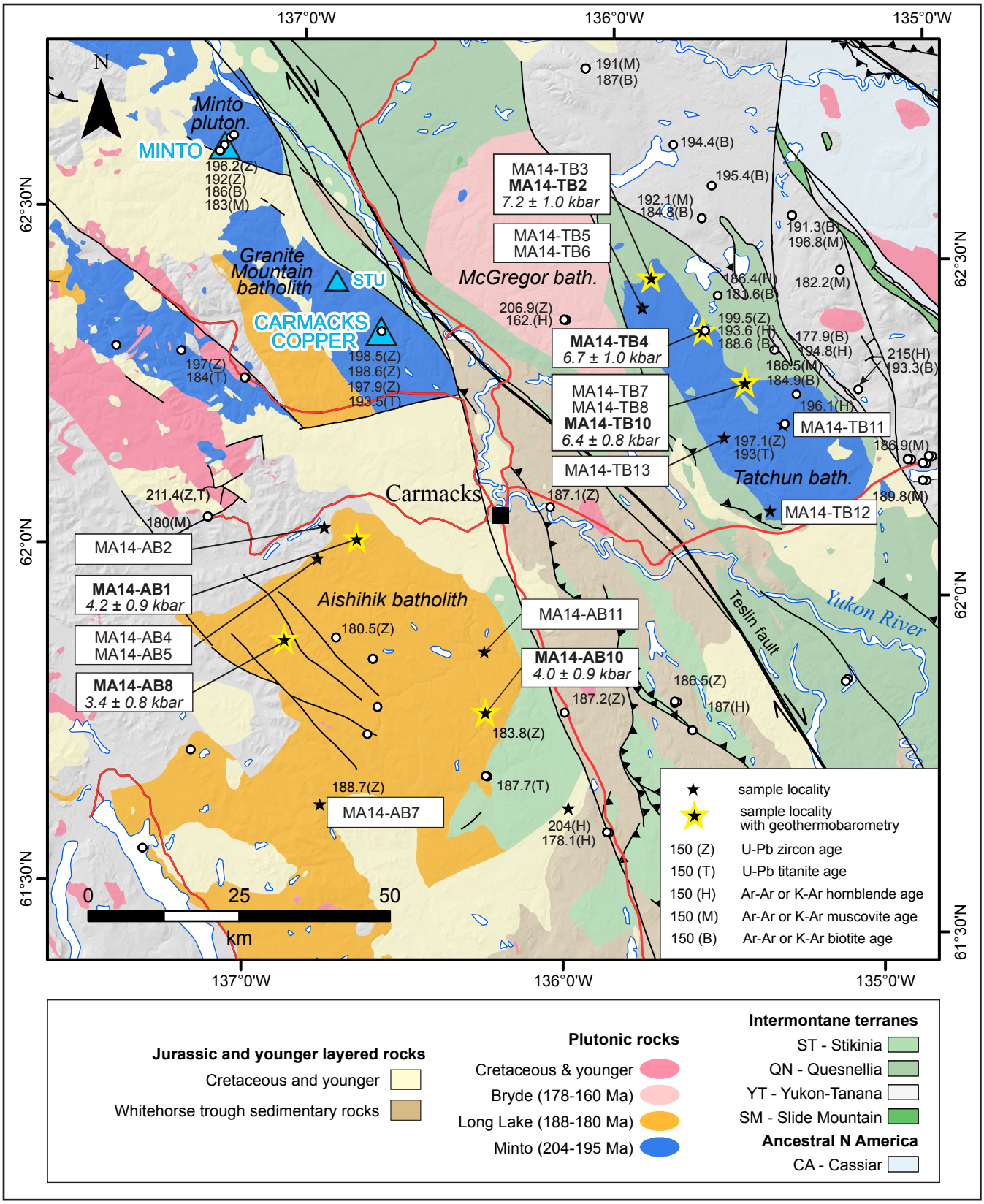

Figure 2. *Simplified geologic map of the study area, indicating published geochronological data from Late Triassic to Middle Jurassic. Sources of geochronological data: Breitsprecher and Mortensen (2004); Colpron (2011); Joyce et al. (2015, 2016). Geological data from Yukon Geological Survey (2015).*

the influence of temperature (*T*) by Anderson and Smith (1995), by taking into account the temperature-dependent equilibria between amphibole and plagioclase (Blundy and Holland, 1990; Holland and Blundy, 1994).

The temperature-corrected Al-in-hornblende geobarometer (referred to herein as "Al-in-hornblende geothermobarometer") was previously applied by McCausland *et al.* (2002) and Tafti (2005) to samples of the Minto pluton and Granite Mountain batholith. Crystallization pressures in the Minto pluton were in the range of 6.1-6.6 kbar (Tafti, 2005), equivalent to ~22-24 km depth under a lithostatic crustal column of 2800 kg/m^3 density. McCausland *et al.* (2002) indicate two spatially separate hornblende populations in the Granite Mountain batholith, with more aluminous, higher-pressure hornblende in the east (5.6-6.6 kbar) and less aluminous, lower-pressure hornblende in the west (4.9-5.8 kbar). Recent investigations (Colpron and Sack, unpublished mapping and data) indicate that the batholith has an eastern lobe composed of older and more deeply exhumed Minto suite granitoid rocks, and a western lobe composed of substantially younger Long Lake suite granitoid rocks (Figs. 1 and 2).

Geobarometric constraints from hornblende and magmatic epidote led Tafti (2005) to conclude that batholiths that post-dated mineralization and deformation at Minto and Carmacks Copper were emplaced at a depth of greater than 20 km. Therefore, Minto and Carmacks Copper deposits are interpreted by Tafti (2005) to represent porphyry systems that formed at shallower crustal depths of a few kilometres, but which were subsequently tectonically buried, deformed, incorporated into intrusions at depth, and subsequently exhumed, all within a few million years. Hood (2012) interprets that the Minto deposit instead formed from magmatic-hydrothermal fluids that focused into active brittle-ductile shear zones in the mid-crust, bypassing the requirement for tectonic burial of shallowly formed mineralization.

A previous study of the Aishihik batholith by Johnston *et al.* (1996) indicates a likely depth of magma emplacement of greater than 30 km. This constraint is based on the regular occurrence of magmatic epidote and a greater than 8 kbar metamorphic assemblage of sillimanite-kyanite-staurolite in pelitic country rocks. Johnston *et al.* (1996) suggests extremely rapid exhumation of the Aishihik batholith to explain melt crystallization at 186.0±2.8 Ma (U-Pb zircon), followed by cooling through ~600°C by 184-185 Ma, as indicated by U-Pb titanite ages.

SAMPLES

A suite of 19 granitoid samples of the Aishihik and Tatchun batholiths were collected during helicopter-supported fieldwork in 2014 (Table 1; Figs. 1 and 2). Cut and hydrofluoric acid-etched rock slabs were stained with sodium cobaltinitrite to identify K-feldspar and with amaranth red to identify plagioclase. Modal mineralogy and rock names were derived from stained slab observations and by petrographic investigations of polished thin sections (Table 1). The Aishihik batholith samples include medium to coarse-grained granodiorite, K-feldspar-phyric granodiorite, granite, aplitic granite and tonalite. The 11 Tatchun batholith samples include K-feldspar-phyric quartz diorite, pegmatitic diorite, K-feldspar-phyric quartz monzonite, quartz monzonite, granodiorite, quartz monzodiorite and aplitic granite.

Samples were first screened for their igneous mineral assemblages; six (three from each of the Aishihik and Tatchun batholiths) were determined to have the requisite equilibrium assemblage of quartz, plagioclase, orthoclase, hornblende, biotite, magnetite (or ilmenite), titanite, melt and vapour, to satisfy the thermodynamic requirements of the Al-in-hornblende geobarometer (Hammarstrom and Zen, 1986). These samples ranged in composition from granodiorite to tonalite to quartz diorite. Hornblende-plagioclase grain boundaries, on each of the six samples, were scrutinized for alteration by transmitted light petrography and scanning electron microscopy (SEM). Only hornblende and plagioclase grains that were texturally intergrown were considered for analysis (Fig. 3). Samples in which hornblende was euhedral or where co-precipitation of hornblende and plagioclase could not be petrographically satisfied were avoided.

Epidote is present in 16 of the 19 samples, including all six of the samples selected for geothermobarometry. In 15 of these, epidote occurs as anhedral replacements of biotite or hornblende, and therefore, is interpreted as a product of deuteric alteration. However, one Tatchun batholith sample (MA14-TB6) contains magmatic epidote as elongate, prismatic, euhedral grains in textural association with, but not replacing hornblende.

METHODOLOGY

Amphibole and plagioclase compositions were determined by electron microprobe analysis (EMPA) at the Electron Microbeam/X-ray Diffraction Facility in the Department of Earth, Ocean, and Atmospheric Sciences at the University

Table 1. *Sample descriptions and locations.*

Sample	Latitude (NAD83)	Longitude (NAD83)	Description	QAP norm (vol.%)			QAP
				K-feldspar	Plagioclase	Quartz	Rock Type
Aishihik batholith							
MA14-AB1*	62.03821	-136.72737	pale pink weathering; fresh grey-pink; weakly foliated, medium-grained sparesely Kfs-porphyritic biotite granodiorite, cut by minor aplite dikes	12	59	29	granodiorite
MA14-AB2	62.05304	-136.83230	tan-weathering 2m-wide aplite dike (cutting biotite orthogneiss)	41	18	41	granite
MA14-AB4	62.00563	-136.84785	fine-grained leucogranite (cutting foliated biotite granite)	38	21	41	granite
MA14-AB5	62.00563	-136.84785	medium-grained foliated biotite granite (cut by fine-grained leucrogranite)	29	41	29	granite
MA14-AB7	61.64092	-136.78826	buff-pink weathering; fine- to medium-grained equigranular, moderately chloritized biotite-hornblende(?) granite	41	18	41	granite
MA14-AB8*	61.88171	-136.93471	white weathering; white fresh; coarse-grained, weakly to moderately foliated, Kfs-porphyritic biorite-hornblende granodiorite	22	44	33	granodiorite
MA14-AB10*	61.79234	-136.28922	weakly foliated, medium-grained hornblende tonalite; accessory titanite and epidote	6	71	24	tonalite
MA14-AB11	61.88325	-136.30288	fine to medium-grained, massive, equigranular hornblende-biorite granite; euhedral 4-6mm biotite grains	21	37	42	granite
Tatchun batholith							
MA14-TB2*	62.45180	-135.82699	white weathering; weakly foliated medium-grained hornblende quartz diorite	6	88	6	quartz diorite
MA14-TB3	62.45180	-135.82699	white weathering; pegmatite leucodiorite	5	94	1	diorite
MA14-TB4*	62.37656	-135.66535	moderately epidotized hornblende phyric quartz diorite (cut by pegmatite leucodiorite)	6	88	6	quartz diorite
MA14-TB5	62.40720	-135.86282	foliated K-feldspar porphyritic medium-grained biotite-hornblende quartz monzonite (cut by fine-grained equigranular granodiorite and granite pegmatite)	44	39	18	quartz monzonite
MA14-TB6	62.40720	-135.86282	fine-grained equigranular granodiorite (cutting foliated bt-hbl granodiorite; cut by granite pegmatite)	13	56	31	granodiorite
MA14-TB7	62.30312	-135.52239	grey, foliated, medium-grained epidotized hornblende quartz diorite	6	88	6	quartz diorite
MA14-TB8	62.30312	-135.52239	hornblende quartz monzodiorite	25	67	8	quartz monzodiorite
MA14-TB10*	62.30312	-135.52239	unfoliated medium-grained hornblende quartz diorite	2	91	8	quartz diorite
MA14-TB11	62.24422	-135.39588	fine-grained equigranular leucogranite	35	24	40	granite (dike)
MA14-TB12	62.11541	-135.42423	K-feldspar porphyritic (5 - 40 mm) medium-grained biotite quartz monzonite; rare fine-grained mafic xenoliths	32	53	16	quartz monzonite
MA14-TB13	62.22087	-135.57949	white weathering; medium-grained equigranular hornblende biotite quartz monzonite	36	46	18	quartz monzonite

Notes:
* denotes sample selected for geothermobarometry

of British Columbia on a fully-automated CAMECA SX-50 instrument operating in wavelength-dispersion mode. For both minerals, the instrument operated with an excitation voltage of 15 kV, beam current of 20 nA, peak count time of 20 s (except 40 s for F in amphibole), background count time of 10 s (except 20 s for F in amphibole), and a spot diameter of 5 μm.

For the elements considered in feldspar, the following standards, X-ray lines and crystals were used: albite, NaKα, thallium acid phthalate (TAP); anorthite, AlKα, TAP; diopside, MgKα, TAP; anorthite, SiKα, TAP; orthoclase, KKα, pentaerythritol (PET); anorthite, CaKα, PET; synthetic rhodonite, MnKα, lithium fluoride (LIF); and synthetic fayalite, FeKα, LIF. For the elements considered in hornblende, the following standards, X-ray lines and crystals were used: synthetic phlogopite, FKα, TAP; albite, NaKα, TAP; kyanite, AlKα, TAP; diopside, MgKα, TAP; diopside, SiKα, TAP; scapolite, ClKα, PET; orthoclase, KKα, PET; diopside, CaKα, PET; rutile, TiKα, PET; synthetic magnesiochromite, CrKα, LIF; synthetic rhodonite, MnKα, LIF; synthetic fayalite, FeKα, LIF; and synthetic Ni_2SiO_4, NiKα, LIF. Data were reduced according to the 'PAP' $\phi(\rho Z)$ method of Pouchou and Pichoir (1985).

Four to six unaltered hornblende-plagioclase grain boundary locations were selected from each of the geothermobarometric samples; for each grain pair, two to four points per hornblende and plagioclase grain rim were analyzed. Rim spots were selected within a few tens of microns of grain boundaries, and additional spot analyses in grain cores were carried out to test for possible alteration or compositional zoning effects. In all cases, core compositions are within the variance of rim compositions, but only rim compositions were used for *P-T* calculations.

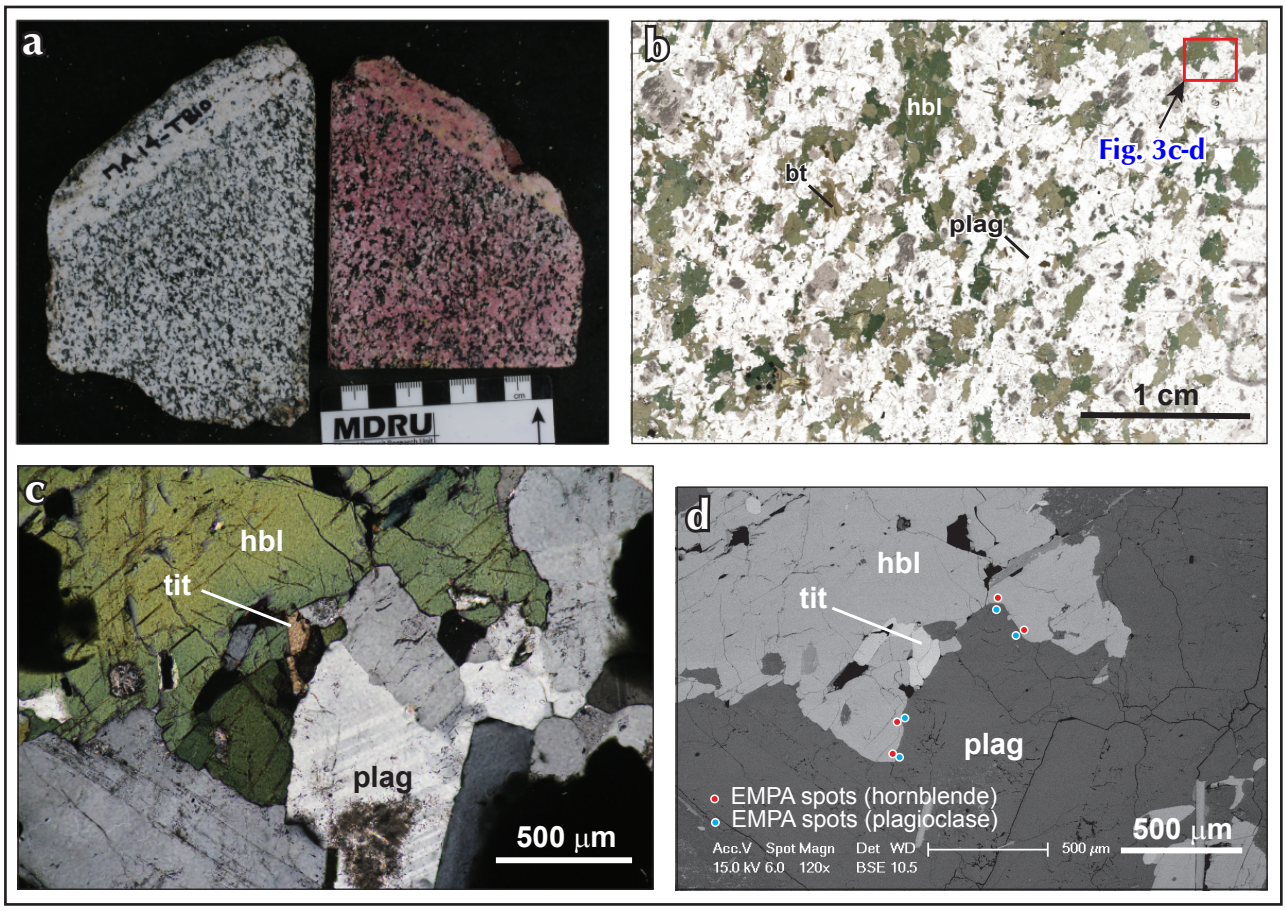

Figure 3. *Sequence of images for hornblende quartz diorite from the Tatchun batholith (MA14-TB10): (a) cut slabs, both unstained (left) and stained sequentially with amaranth red (for plagioclase) and sodium cobaltinitrite (for K-feldspar; right); (b) polished thin section of same sample, showing the location of a hornblende-plagioclase grain pair for EMPA analysis (red box); (c) cross-polarized microphotograph showing intergrown hornblende-plagioclase grain boundary; (d) backscattered electron image of (c), showing the location of EMPA points along grain rims of hornblende (red dots) and plagioclase (blue dots). Mineral abbreviations: bt=biotite; hbl=hornblende; plag=plagioclase; tit=titanite.*

Electron microprobe analyses of amphibole rims (Appendix A) were converted to amphibole formulae (Table 2) using the routine of Holland and Blundy (1994). All hornblende grains analyzed are calcic and range from hastingsitic to Mg-hastingsitic in Tatchun samples and Mg-hastingsitic to edenitic in Aishihik samples (Table 2). Within-grain variability is generally significantly greater than analytical uncertainty for the main mineral-forming elements, so the standard deviation of element concentrations among EMPA points is used to estimate the compositional uncertainty of a given mineral grain (Table 2).

A rigorous approach was used to determine the error in the aluminum content of hornblende, applying the same statistical technique commonly used for establishing error-weighted mean ages in geochronological analysis (Appendix B; Ludwig, 2008). For each hornblende grain, an inverse-variance weighted mean wt% Al_2O_3 was determined, and if the probability-of-fit was above 0.15, the error was derived from the internal (analytical) errors. If the probability-of-fit was below 0.15, the error was calculated as the product of the Student's t-value and the square root of the mean square weighted deviation. For a given rock sample, a mean wt% Al_2O_3 for all the hornblende grains analyzed was determined using the same routine, yielding a single hornblende composition and statistically robust error determination. The relative error in the total Al content (Al^{TOT}) of the hornblende composition is ~1% for most samples.

Mineral composition data were validated against the allowable plagioclase and hornblende compositional ranges for which the hornblende-plagioclase geothermobarometer has been calibrated. In all samples, the average ratio of ferric Fe to total Fe (Fe^{3+}#) is above the requisite value of 0.25, and the average Fe number (Fe# = Fe*/(Mg + Fe*)) is between the allowable range of 0.40 and 0.65 (Anderson and Smith, 1995). These requirements are critical given that low oxygen fugacity results in over-estimation of crystallization pressure (Anderson and Smith, 1995). The mole fraction of anorthite in plagioclase is between An_{15} and An_{38}, somewhat greater than the range of An_{25} and An_{35} typically applied for Al-in-hornblende geothermobarometry (*e.g.*, Anderson and Smith, 1995).

Temperatures of crystallization were calculated using the edenite + albite = richterite + anorthite mineral thermometer of Holland and Blundy (1994; Table 2), and pressures of crystallization were calculated according to the geothermobarometer of Anderson and Smith (1995):

$$P\ (\pm 0.6\ \text{kbar}) = 4.76\ Al^{TOT} - 3.01 - \{(T - 675)/85\} \times \{0.530\ Al^{TOT} + 0.005294(T - 675)\} \quad \text{(Equation 1)}$$

where T is the temperature of crystallization in °C and Al^{TOT} is the total aluminum content of hornblende. Calculations were performed using an MS Excel spreadsheet prepared by J.L. Anderson that was obtained from R. Tafti (pers. comm., 2014). For the mean hornblende and plagioclase compositions of a given sample, *P-T* conditions were calculated iteratively using an initial *P-T* condition calculated with equations in Schmidt (1992) and Holland and Blundy (1994). All pressure results are well above the lower 2 kbar calibration limit of Anderson and Smith's (1995) geothermobarometer.

The temperature-sensitivity of the Al-in-hornblende geobarometer is well-documented (*e.g.*, Anderson and Smith, 1995), so multiple mineral geothermometers were tested. The alternative edenite + 4 quartz = tremolite + albite geothermometer (Blundy and Hollard, 1990; Holland and Blundy, 1994) returned temperatures that were 20-170°C higher than those obtained with the edenite + albite = richterite + anorthite geothermometer (above). A possible explanation for the discrepancy is that quartz may have precipitated late in the crystallization sequence in the Aishihik and Tatchun batholith samples, and was not actually involved in the exchange of components between plagioclase and amphibole. The Ti-in-hornblende geothermometer of Otten (1984) was tested as an alternative, but yielded consistently low temperatures, potentially arising from exsolution of a Ti-bearing phase from amphibole during cooling (Ernst and Liu, 1998). Although petrographic observations support an equilibrium assemblage of quartz, plagioclase, orthoclase, hornblende, biotite, magnetite and titanite in all samples analyzed, it is cautioned that deviations from an equilibrium condition affect the quantitative validity of our *P* and *T* calculations.

Table 2. *Summary of average hornblende compositions.*

Sample		Aishihik batholith			Tatchun batholith		
		MA14-AB1	MA14-AB8	MA14-AB10	MA14-TB2	MA14-TB4	MA14-TB10
SiO_2	%	43.00	45.00	42.34	40.00	38.51	40.44
TiO_2	%	0.85	0.82	0.96	0.94	1.04	0.80
Al_2O_3	%	9.66	7.86	10.00	12.82	13.28	11.70
FeO*	%	18.47	17.13	18.32	18.89	21.17	20.41
MgO	%	10.12	11.35	10.01	8.89	7.18	8.24
MnO	%	0.82	0.74	0.74	0.33	0.48	0.50
CaO	%	11.58	11.40	11.49	10.62	10.50	11.16
Na_2O	%	1.16	1.26	1.11	2.61	2.58	1.82
K_2O	%	1.10	0.90	1.20	1.47	1.66	1.62
F	%	0.40	0.41	0.24	0.22	0.16	0.22
Cl	%	0.04	0.02	0.05	0.01	0.01	0.03
Sum	%	97.21	96.88	96.45	96.79	96.57	96.92
Element	**Site[a]**						
Si	T	6.485	6.756	6.425	6.124	5.982	6.224
Al^{IV}	T	1.515	1.244	1.575	1.876	2.018	1.776
Al^{VI}	M1,2,3	0.202	0.147	0.215	0.437	0.414	0.346
Ti	M1,2,3	0.097	0.092	0.109	0.108	0.121	0.093
Fe^{3+}	M1,2,3	0.813	0.656	0.831	0.610	0.738	0.661
Mg	M1,2,3	2.274	2.539	2.263	2.028	1.662	1.891
Mn	M1,2,3	0.104	0.095	0.095	0.042	0.063	0.065
Fe^{2+}	M1,2,3	1.510	1.471	1.487	1.774	2.002	1.944
Fe^{2+}	M4	0.007	0.024	0.008	0.035	0.011	0.022
Ca	M4	1.872	1.834	1.869	1.742	1.748	1.840
Na	M4	0.122	0.142	0.123	0.224	0.241	0.139
Na	A	0.218	0.226	0.203	0.550	0.535	0.404
K	A	0.211	0.172	0.231	0.287	0.330	0.319
OH	OH	1.794	1.799	1.873	1.890	1.918	1.886
F	OH	0.197	0.196	0.115	0.106	0.079	0.107
Cl	OH	0.010	0.005	0.012	0.004	0.003	0.007
Sum cations		15.429	15.398	15.434	15.837	15.865	15.722
Al^{TOT}	%	1.717	1.391	1.790	2.314	2.432	2.122
$Fe^{3+}\#$[b]		0.349	0.305	0.357	0.252	0.268	0.252
Fe#[c]		0.506	0.459	0.507	0.544	0.623	0.581
Amphibole type:		Mg-hastingsite	edenite	Mg-hastingsite	Mg-hastingsite	hastingsite	hastingsite

Notes:
[a] Amphibole sites: T = tetrahedral; M1,2,3 = octahedral; M4 = large octahedral; A = alkali vacancies; OH = anionic
[b] $Fe^{3+}\# = Fe^{3+}/Fe^*$
[c] $Fe\# = Fe^*/(Mg + Fe^*)$

RESULTS - GEOTHERMOBAROMETRY

The *P-T* conditions of crystallization and corresponding lithostatic emplacement depths have been calculated for the Aishihik and Tatchun batholith samples and are presented in Table 3. To assess the statistical significance of these calculated values, three sources of error are considered: (a) the approximate ±0.6 kbar regression error associated with uncertainties in the *P-T* correlation of the Anderson and Smith (1995) geothermobarometer; (b) the error associated with the input variable Al^{TOT}, which itself is a function of analytical precision and both within-grain and between-grain variability (Appendix B); and (c) uncertainty in the temperature of crystallization, which can be estimated from uncertainty in plagioclase compositions. The error in pressure arising from uncertainties in Al^{TOT} and *T* was propagated from known errors of the input variables in Equation 1, which yielded a combined error $\sigma_{Al,T}$ of ±0.23 to ±0.37 kbar. An estimate of the total error σ_{TOT} is given by the sum of the regression error (σ_{REG}) and propagated Al and *T* errors, and is between ±0.8 to ±1.0 kbar for all samples (13-24% error, equivalent to ±3.0 to ±3.5 km). All quoted errors are at the 1σ level of uncertainty, but a more conservative ±1.6 to ±2.0 kbar error at the 2σ level is perhaps more appropriate, especially if one considers other possible sources of error in the temperature estimate (*e.g.*, there is a ±0.8 kbar error associated with a ±50°C temperature uncertainty; Anderson and Smith, 2005).

Nevertheless, samples of the Aishihik and Tatchun batholiths define two statistically distinct pressure/depth regimes (Fig. 4). Aishihik samples range from 3.4-4.2 kbar (12-15 km), whereas Tatchun samples are consistently higher pressure at 6.4-7.2 kbar (23-26 km). Re-calculated *P-T* conditions of crystallization using the EMPA data of McCausland *et al.* (2002) and Tafti (2005) indicate that the broadly coeval Tatchun batholith, Minto pluton, and eastern Granite Mountain batholith (Minto suite) were emplaced at similar crustal depths of ~20-26 km, whereas magmas of the Long Lake suite in the Aishihik batholith were emplaced at distinctly shallower levels (~12-15 km). The broadly coeval western part of the Granite Mountain batholith was emplaced at somewhat greater depths of ~18-21 km (McCausland *et al.*, 2002).

Table 3. *Geothermobarometry results.*

Sample	Plagioclase X_{An} [a]	±1σ [b]	Amphibole Al^{TOT}	±1σ [c]	T (°C)	±1σ [d]	P (kbar)	±1σ_{REG} [e]	±1σ_{Al} [f]	±1σ_{T} [g]	±1$\sigma_{Al,T}$ [h]	±1σ_{TOT} [i]	Depth (km)	±1σ [j]
Aishihik Batholith														
MA14-AB1	0.320	0.028	1.717	0.034	**734**	10	**4.18**	0.6	0.16	0.19	0.31	0.91	**15.2**	3.3
MA14-AB8	0.213	0.015	1.391	0.014	**694**	7	**3.42**	0.6	0.07	0.07	0.23	0.83	**12.4**	3.0
MA14-AB10	0.377	0.036	1.790	0.006	**764**	12	**4.03**	0.6	0.03	0.27	0.31	0.91	**14.7**	3.3
Tatchun Batholith														
MA14-TB2	0.147	0.028	2.314	0.015	**724**	15	**7.15**	0.6	0.07	0.16	0.37	0.97	**26.0**	3.5
MA14-TB4	0.187	0.037	2.432	0.024	**765**	17	**6.69**	0.6	0.12	0.44	0.37	0.97	**24.4**	3.5
MA14-TB10	0.206	0.019	2.122	0.019	**721**	8	**6.36**	0.6	0.08	0.15	0.23	0.83	**23.1**	3.0

Notes:
[a] X_{An} refers to mole fraction of anorthite component in plagioclase
[b] error in plagioclase composition is estimated from the standard deviation of plagioclase compositions (both within-grain and between-grain)
[c] error in Al^{TOT} is calculated from the 1σ error in Al_2O_3 (Appendix)
[d] error in *T* is propagated from the error in the plagioclase composition (at fixed hornblende composition)
[e] σ_{REG} refers to the approximate 1σ regression error of the Anderson and Smith (1995) geothermobarometer
[f] σ_{Al} refers to the 1σ error in pressure due to uncertainty in the Al^{TOT}
[g] σ_{T} refers to the 1σ error in pressure due to uncertainty in crystallization temperature
[h] $\sigma_{Al,T}$ is the propagated 1σ error in pressure due to errors in Al^{TOT} and *T*
[i] σ_{TOT} is the estimated total error in pressure calculated by adding the regression error and propagated (Al^{TOT} and *T*) errors
[j] error in depth taking into account the combined uncertainty in pressure (σ_{TOT})

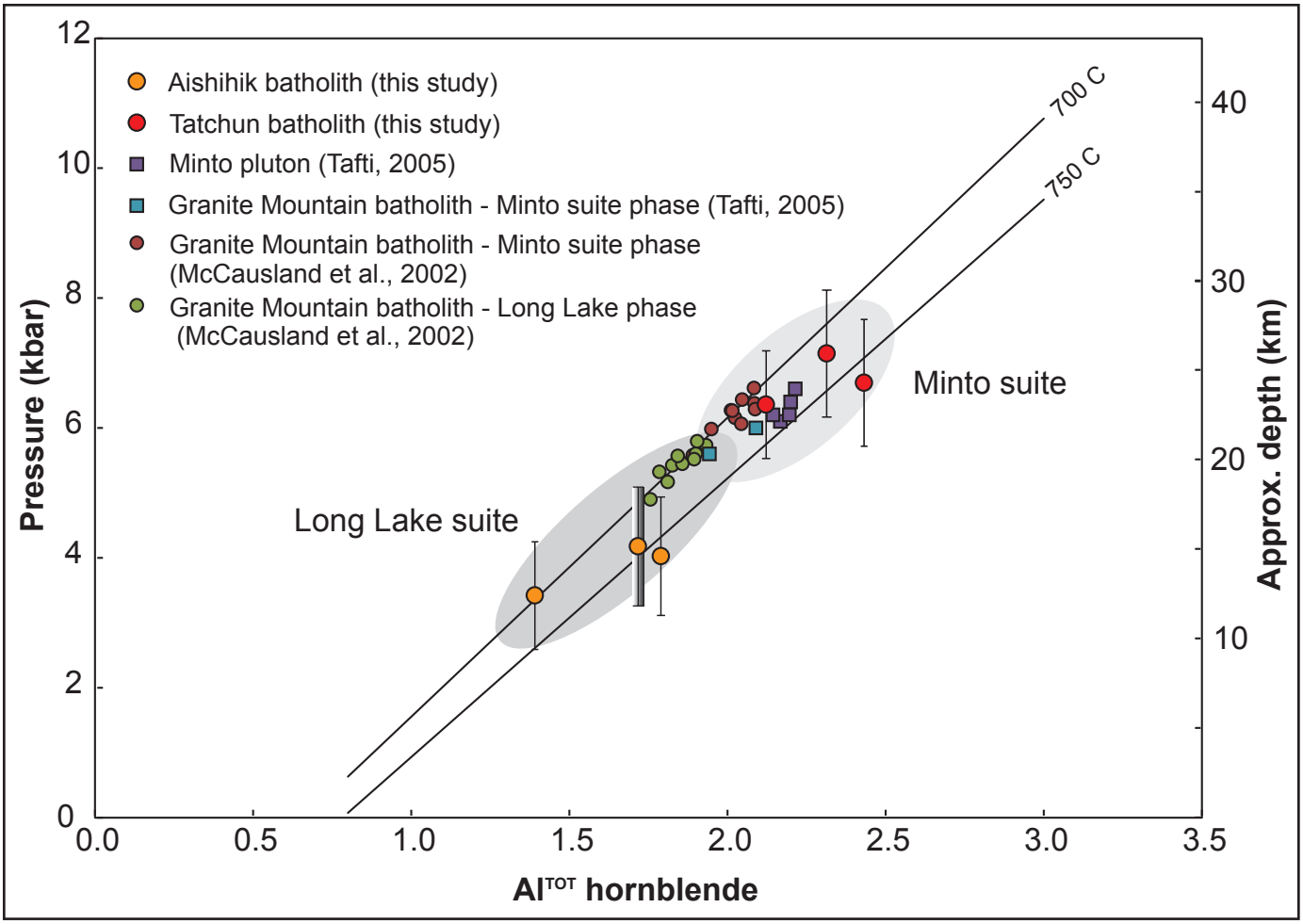

Figure 4. *Plot showing the relationship between Al^{TOT} in hornblende and calculated pressures and depths (at 2800 kg/m^3). Error bars represent 1σ_{TOT} uncertainty in pressure and errors in Al^{TOT} are less than the symbol width. Data from McCausland et al. (2002) and Tafti (2005) are included for comparison (errors omitted for clarity). Samples from the Minto suite (pale grey ellipse) were emplaced at systematically higher pressure than those of the Long Lake suite (medium grey ellipse).*

DISCUSSION

Geothermobarometric results indicate that the Tatchun batholith was emplaced at a depth of approximately 23 to 26 km, which is consistent with the pressure/depth estimates of Tafti (2005) and McCausland *et al.* (2002) for the age-equivalent Minto pluton and eastern part of the Granite Mountain batholith (Figs. 1 and 2). Following crystallization of the Tatchun batholith *ca.* 200-197 Ma, magmatic biotite records an Ar-Ar cooling age of 188.6 ± 1.1 Ma (Colpron, 2011; Joyce *et al.*, 2015). Assuming that the biotite age is the result of regional cooling through ~300°C, and with an average geothermal gradient of ~30°C/km, the Tatchun batholith was exhumed to ~10 km depth within 8 to 11 m.y. of emplacement. Therefore, Tatchun batholith's average exhumation rate over this time was ~1.2-2.0 mm/a. At a constant exhumation rate, the batholith would have been exposed at surface by ~184-180 Ma.

The ~1.2-2.0 mm/a rate of exhumation estimated for the Tatchun batholith is modest given higher rates of erosion in active collisional orogens. For example, the St. Elias Mountains in southwest Yukon, which are currently being uplifted due to collision of the Yakutat block with the western margin of North America in southeast Alaska since approximately 10-5 Ma, are undergoing rates of erosion of 5.1 mm/a (Sheaf *et al.*, 2003). In the

northwestern Himalayas, Indus river bedrock incision rates as equated to bedrock uplift rates during the Quaternary range from 2 to 12 mm/a (Burbank *et al.*, 1996). Furthermore, thermochronometric measurements along a segment of the Alpine fault in the Southern Alps of New Zealand indicate vertical exhumation rates ranging from 6-9 mm/a (Little *et al.*, 2005). Therefore, Early Jurassic exhumation rates in the Cordilleran orogen need not have been exceptional by global standards.

The Aishihik batholith crystallized between 188 and 180 Ma (Joyce *et al.*, 2016) and at depths of ~12 to 15 km – significantly shallower than plutons of the Minto suite. Results of this study differ markedly from the Johnston *et al.* (1996) interpretation that the Aishihik batholith was emplaced in excess of 30 km. The discrepancy could be due to emplacement of the batholith well after, and at shallower crustal level than the peak metamorphic conditions responsible for the sillimanite-kyanite-staurolite assemblage in pelite west of the batholith.

Perhaps the best control on exhumation of the Aishihik batholith is given by a 185.9±2.0 Ma U-Pb zircon age on a porphyritic phase of the batholith (sample MA14-AB9; Joyce *et al.*, 2016). The very fine grained matrix of the sample is typical of upper crustally emplaced (<10 km?), structurally controlled intrusions emanating from an underlying, fluid-saturated magma chamber. Elsewhere in the batholith, miarolitic cavities and dikes of granitic pegmatite and aplite are direct evidence of fluid exsolution, which is favoured at shallower levels in the crust due to the lower solubility of water in silicate melt at lower pressure. Although the pressure or depth of these features cannot be constrained, field relationships are reasonably explained by unroofing of the batholith during the 8 m.y. magmatic timespan of the Aishihik batholith.

K-Ar biotite cooling ages in the Aishihik batholith range from 170 to 164 Ma (Johnston *et al.*, 1996; Breitsprecher and Mortensen, 2004), indicating that parts of the batholith had cooled below ~300°C by this time. At an assumed geothermal gradient of 30°C/km, interpretation of K-Ar data would imply that the batholith was still at ~10 km depth 10 to 16 m.y. after final crystallization around 180 Ma. Therefore, if exhumation was rapid during the 188-180 Ma window of batholith emplacement, exhumation likely tapered off or stalled by the Middle Jurassic. This interpretation is consistent with the waning of regional cooling by Middle to Late Jurassic over much of Yukon's Cordilleran hinterland (Colpron, 2011; Allan *et al.*, 2013; Nelson *et al.*, 2013).

CONCLUSIONS

This study establishes that the earliest Jurassic Tatchun batholith of the Minto suite (200-197 Ma) was emplaced at a depth of ~23 to 26 km, similar to that previously proposed for the Minto pluton and Granite Mountain batholith. Geochronological and thermal constraints suggest that the Tatchun batholith likely exhumed at a reasonably modest rate of ~1.2-2.0 mm/a, although additional data from the Tatchun and other Minto suite plutons are required.

The Aishihik batholith of the Long Lake suite (188-180 Ma) was emplaced at a crustal depth of ~12 to 15 km, which contrasts strongly with the greater than 30 km estimate of Johnston *et al.* (1996). Crosscutting porphyritic and fluid-saturated phases of the Aishihik batholith are reasonably explained by exhumation of the batholith to shallower (<10 km?) depths during the ~8 my duration of magmatism. Exhumation rates slowed dramatically after magmatism ceased, as indicated by Middle Jurassic K-Ar biotite cooling ages.

Minto suite plutons are deeply unroofed and therefore unprospective for coeval subvolcanic porphyry copper deposits (*e.g.*, Chapman, 2014). However, the Minto and Carmacks Copper Cu-Au-Ag deposits are evidence that these plutons are prospective for somewhat older, deformed mineralization, which formed or was metamorphosed at deep magmatic levels. In contrast, fluid-saturated and hypabyssal phases of the Aishihik batholith suggest a magmatic environment permissible for magmatic-hydrothermal mineralization.

Additional geothermobarometric studies of various other Late Triassic to Early Jurassic plutons will be integrated with geochronological studies of the same intrusions to further resolve the evolution of magmatism and structure during this important stage of Cordilleran tectonics.

ACKNOWLEDGEMENTS

This contribution builds on a University of British Columbia BSc Honours project by MJT, which was supported by the Yukon-Alaska Metallogeny Project – a research partnership between the Mineral Deposit Research Unit, Yukon Geological Survey, Kaminak Gold Corp., and Sumac Mines Ltd. This study contributes to a comprehensive characterization study of Late Triassic to Early Jurassic plutonic suites in Yukon by the Yukon Geological Survey and Geological Survey of Canada.

REFERENCES

Allan, M.M., Mortensen, J.K., Hart, C.J.R., Bailey, L.A., Sanchez, M.G., Ciolkiewicz, W., McKenzie, G.G. and Creaser, R.A., 2013. Magmatic and metallogenic framework of west-central Yukon and eastern Alaska. *In*: Tectonics, Terranes, Metallogeny and Discovery in the northern circum-Pacific region, M. Colpron, T. Bissig, B. Rusk and J. Thompson (eds.), Society of Economic Geologists, Special Publication vol. 17, p. 111-168.

Anderson, J.L. and Smith, D.R., 1995. The effects of temperature and fO2 on the Al-in hornblende barometer. American Mineralogist, vol. 80, p. 549-559.

Blundy, J.D. and Holland, T.J.B., 1990. Calcic amphibole equilibria and a new amphibole-plagioclase geothermometer. Contributions to Mineralogy and Petrology, vol. 104, p. 208-224.

Breitsprecher, K. and Mortensen, J.K. (compilers), 2004. YukonAge 2004: A database of isotopic age determinations for rock units from Yukon Territory. Yukon Geological Survey (CD-ROM).

Buffett, G., White, D., Roberts, B. and Colpron, M., 2006. Preliminary results from the Whitehorse Trough seismic survey, Yukon Territory. Geological Survey of Canada, Current Research 2006-A2, 9 p.

Burbank, D.W., Leland, J., Fielding, E., Anderson, R.S., Brozovic, N., Reid, M.R. and Duncan, C., 1996. Bedrock incision, rock uplift and threshold hillslopes in the northwestern Himalayas. Nature, vol. 379, p. 505-510.

Chapman, J.B., 2014. Are there elephants hiding in the Early Jurassic of Yukon? A tectono-magmatic perspective on porphyry prospectivity. *In:* Annual Geological Society of America Meeting in Vancouver British Columbia, Programs with Abstracts, vol. 46, p. 590.

Colpron, M. (compiler), 2011. Geological compilation of Whitehorse trough - Whitehorse (105D), Lake Laberge (105E), and part of Carmacks (115I), Glenlyon (105L), Aishihik Lake (115H), Quiet Lake (105F) and Teslin (105C). Yukon Geological Survey, Geoscience Map 2011-1, 1:250000 scale.

Colpron, M. and Friedman, R.M., 2008. U-Pb zircon ages for the Nordenskiold Formation (Laberge Group) and Cretaceous intrusive rocks, Whitehorse trough, Yukon. *In:* Yukon Exploration and Geology 2007, D.S. Emond, L.R. Blackburn, R.P. Hill and L.H. Weston (eds.), Yukon Geological Survey, p. 139-151.

Colpron, M., Crowley, J.L., Gehrels, G., Long, D.G.F., Murphy, D.C., Beranek, L. and Bickerton, L., 2015. Birth of the northern Cordilleran orogen, as recorded by detrital zircons in Jurassic synorogenic strata and regional exhumation in Yukon. Lithosphere, vol. 7, p. 541-562.

Dickie, J.R. and Hein, F.J., 1995. Conglomeratic fan deltas and submarine fans of the Jurassic Laberge Group, Whitehorse trough, Yukon Territory, Canada - Fore-arc sedimentation and unroofing of a volcanic island-arc complex. Sedimentary Geology, vol. 98, p. 263-292.

Ernst, W.G. and Liu, J.L., 1998. Experimental phase-equilibrium study of Al- and Ti-contents of calcic amphibole in MORB – A semiquantitative thermobarometer. American Mineralogist, vol. 83, p. 952-969.

Fillmore, J.A., 2006. Character and origin of the Lower Jurassic (Pliensbachian) Nordenskiold dacite, Whitehorse trough, Yukon Territory, Canada. Unpublished BSc Honours thesis, Laurentian University, Ontario, 28 p.

Gordey, S.P. and Makepeace, A.J., 2001. Bedrock geology, Yukon Territory. Geological Survey of Canada, Open File 3754, scale 1:1000000; *also Yukon Geological Survey, Open File 2001-1*.

Hammarstrom, J.M. and Zen, E., 1986. Aluminum in hornblende: An empirical igneous geobarometer. American Mineralogist, vol. 71, p. 1297-1313.

Hart, C.J.R., 1997. A Transect across Northern Stikinia: Geology of the Northern Whitehorse Map Area, Southern Yukon Territory (105D/13-16). Exploration and Geological Services Division, Yukon Region, Indian and Northern Affairs Canada, Bulletin 8, 112 p.

Hart, C.J.R., Dickie, J.R., Ghosh, D.K. and Armstrong, R.L., 1995. Provenance Constraints for Whitehorse Trough Conglomerate: U-Pb Zircon Dates and Initial Sr Ratios of Granitic Clasts in Jurassic Laberge Group, Yukon Territory. *In:* Jurassic Magmatism and Tectonics of the North American Cordillera, Geological Society of America Special Paper 299, p. 47-63. doi 10.1130/SPE299-p47.

Holland, T.J.B. and Blundy, J.D., 1994. Non-ideal interactions in calcic amphiboles and their bearing on amphibole-plagioclase thermometry. Contributions to Mineralogy and Petrology, vol. 116, p. 433-447.

Hollister, L.S., Grissom, G.C., Peters, E.K., Stowell, H.H. and Sisson, V.B., 1987. Confirmation of the empirical correlation of Al in hornblende with pressure of solidification of calc-alkaline plutons. American Mineralogist, vol. 72, p. 231-239.

Hood, S.B., 2012. Mid-crustal Cu-Au mineralization during episodic pluton emplacement, hydrothermal fluid flow, and ductile deformation at the Minto deposit, YT, Canada. Unpublished MSc thesis, The University of British Columbia, British Columbia, 220 p.

Johnston, S.T., Mortensen, J.K., and Erdmer, P., 1996. Igneous and metaigneous age constraints for the Aishihik metamorphic suite, southwest Yukon. Canadian Journal of Earth Sciences, vol. 33, p. 1543-1555.

Johnston, S.T. and Canil, D., 2007. Crustal architecture of SW Yukon, northern Cordillera: Implications for crustal growth in a convergent margin orogen. Tectonics, vol. 26, p. 1-18.

Joyce, N.L., Ryan, J.J., Colpron, M., Hart, C.J.R., and Murphy, D.C., 2015. A compilation of $^{40}Ar/^{39}Ar$ age determinations for igneous and metamorphic rocks, and mineral occurrences from central and southeast Yukon; Geological Survey of Canada, Open File 7924, 1 .zip file. doi:10.4095/297446

Joyce, N., Colpron, M., Allan, M.M., Sack, P.J., Crowley, J.L. and Chapman, J.B., 2016. New U-Pb zircon ages from the Aishihik batholith, southern Yukon. *In*: Yukon Exploration and Geology 2015, K.E. MacFarlane and M.G. Nordling (eds.), Yukon Geological Survey, p. 129-147.

Little, T.A., Cox, S., Vry, J.K. and Batt, G., 2005. Variations in exhumation level and uplift rate along the oblique-slip Alpine fault, central Southern Alps, New Zealand. GSA Bulletin, vol. 117, p. 707-723.

Logan, J.M. and Mihalynuk, M.G., 2014. Tectonic controls on Early Mesozoic paired alkaline porphyry deposit belts (Cu-Au ± Ag-Pt-Pd-Mo) within the Canadian Cordillera. Society of Economic Geologists, Economic Geology, vol. 109, p. 827-858.

Lowey, G.W., 2004. Preliminary lithostratigraphy of the Laberge Group (Jurassic), south-central Yukon: Implications concerning the petroleum potential of the Whitehorse trough. *In*: Yukon Exploration and Geology 2003, D.S. Emond, L.L. Lewis (eds.), Yukon Geological Survey, p. 129-142.

Lowey, G.W., 2008. Summary of the stratigraphy, sedimentology and hydrocarbon potential of the Laberge Group (Lower–Middle Jurassic), Whitehorse trough, Yukon. *In*: Yukon Exploration and Geology 2007, D.S. Emond, L.R. Blackburn, R.P. Hill and L.H. Weston (eds.), Yukon Geological Survey, p. 179-197.

Ludwig, K.R., 2008. Isoplot 3.70: A Geochronological Tookit for Microsoft Excel, Berkeley Geochronology Center.

McCausland, P.J.A, Symons, D.T.A., Hart, C.J.R. and Blackburn, W.H., 2002. Paleomagnetism and geobarometry of the Granite Mountain batholith, Yukon: Minimal geotectonic motion of the Yukon-Tanana Terrane relative to North America. *In*: Yukon Exploration and Geology 2001, D.S. Emond, L.H. Weston and L.L. Lewis (eds.), Exploration and Geological Services Division, Yukon, Indian and Northern Affairs Canada, p. 163-177.

McMillan, W.J., Thompson, J.F.H., Hart, C.J.R. and Johnston, S.T., 1995. Regional geological and tectonic setting of porphyry deposits in British Columbia and Yukon Territory. *In*: Porphyry Deposits of the Northwestern Cordillera of North America, T.G. Schroeter (ed.), Canadian Institute of Mining and Metallurgy, Special Volume 46, p. 40-57.

Mercer, B. and Sagman, J., 2012. Phase VI preliminary feasibility study technical report, Minto mine. Minto Explorations Ltd., 368 p. <http://capstonemining.com/i/pdf/PFS.pdf> [accessed December 9, 2012].

Mihalynuk, M.G., Nelson, J.A. and Diakow, L.J., 1994. Cache Creek terrane entrapment: Oroclinal paradox within the Canadian Cordillera. Tectonics, vol. 13, p. 575-595.

Mihalynuk, M.G., Erdmer, P., Ghent, E.D., Cordey, F., Archibald, D.A., Friedman, R.M. and Johannson, G.G., 2004. Coherent French Range blueschist: Subduction to exhumation in <2.5 m.y.? Geological Society of America Bulletin, vol. 116, p. 910-922.

Mira Geoscience, 2014. Geologically-constrained inversion of magnetic and gravity data over parts of the Yukon-Tanana terrane and Whitehorse trough. Yukon Geological Survey, Miscellaneous Report MR-10, Mira Geoscience Project No. 3984, 81 p.

Mortensen, J.K., Emon, K., Johnston, S.T. and Hart, C.J.R., 2000. Age, geochemistry, paleotectonic setting and metallogeny of Late Triassic-Early Jurassic intrusions in the Yukon and eastern Alaska: a preliminary report. *In*: Yukon Exploration and Geology 1999, D.S. Edmond and L.H. Weston (eds.), Exploration and Geological Services Division, Yukon Region, Indian and Northern Affairs Canada, p. 139-144.

Nelson, J.L., Colpron, M. and Israel, S., 2013. The Cordillera of British Columbia, Yukon, and Alaska: Tectonics and Metallogeny. *In*: Tectonics, Terranes, Metallogeny and Discovery in the northern circum-Pacific region, M. Colpron, T. Bissig, B. Rusk and J. Thompson (eds.), Society of Economic Geologists, Special Publication vol. 17, p. 53-109.

Otten, M.T., 1984. The origin of brown hornblende in the Artfjallet gabbro and dolerites. Contributions to Mineralogy and Petrology, vol. 86, p. 189-199.

Pearson, W.N. and Clark, A.H., 1979. The Minto copper deposit, Yukon Territory: A metamorphosed orebody in the Yukon crystalline terrane. Economic Geology, vol. 74, p. 1577-1599.

Pouchou, J.L. and Pichoir, F., 1985. PAP $\phi(\rho Z)$ procedure for improved quantitative microanalysis. Microbeam Analysis, vol. 1985, p. 104-106.

Schmidt, M.W., 1992. Amphibole composition in tonalite as a function of pressure: An experimental calibration of the Al-in hornblende barometer. Contributions to Mineralogy and Petrology, vol. 110, p. 304-310.

Sheaf, M.A., Serpa, L. and Pavlis, T.L., 2003. Exhumation rates in the St. Elias Mountains, Alaska. Tectonophysics, vol. 367, p. 1-11.

Simard, R.L. and Devine, F., 2003. Preliminary geology of the southern Semenof Hills, Yukon (105E/1,7,8). *In*: Yukon Exploration and Geology 2002, D.S. Emond and L.L Lewis (eds.), Exploration and Geological Services Division, Yukon Region, Indian and Northern Affairs Canada, p. 213-222.

Tafti, R., 2005. Nature and origin of the Early Jurassic copper (-gold) deposits at Minto and Williams Creek, Carmacks Copper Belt, western Yukon: Examples of deformed porphyry deposits. Unpublished MSc thesis, The University of British Columbia, British Columbia, 213 p.

Tafti, R. and Mortensen, J.K., 2004. Early Jurassic porphyry-copper (-gold) deposits at Minto and Williams Creek, Carmacks copper belt, western Yukon. *In*: Yukon Exploration and Geology 2003, D.S. Emond and L.L. Lewis (eds.), Yukon Geological Survey, p. 289–303.

Tempelman-Kluit, D.J., 1984. Geology, Laberge (105E) and Carmacks (105I), Yukon Territory. Geological Survey of Canada, Open File 1101, 1:250 000 scale.

Tempelman-Kluit, D.J., 2009. Geology of Carmacks and Laberge map areas, central Yukon: Incomplete draft manuscript on stratigraphy, structure and its early interpretation (ca. 1986). Geological Survey of Canada, Open File 5982, 399 p.

White, D., Colpron, M. and Buffett, G., 2012. Seismic and geological constraints on the structure of the northern Whitehorse trough, Yukon, Canada. Bulletin of Canadian Petroleum Geology, vol. 60, p. 239-255.

Yukon Geological Survey, 2015. Yukon Digital Bedrock Geology, <ftp://ftp.geomaticsyukon.ca/GeoYukon/Geological/>, [accessed November 15, 2015].

Yukon MINFILE, 2015. Yukon MINFILE - A database of mineral occurrences. Yukon Geological Survey, <http://data.geology.gov.yk.ca> [accessed November 30, 2015]

Zen, E. and Hammarstrom, J.M., 1984. Magmatic epidote and its petrologic significance. Geology, vol. 12. p. 515-518.

APPENDIX A. *Hornblende EMPA results (summary results per grain).*

	SiO_2	TiO_2	Al_2O_3	FeO*[a]	MgO	MnO	CaO	Na_2O	K_2O	F	Cl	Sum
average RSD (%):	**0.39**	**3.6**	**0.66**	**0.93**	**0.81**	**7.2**	**0.76**	**3.0**	**2.4**	**47**	**48**	
Grain (no. analyses)	**MA14-AB1 (Aishihik batholith)**											
B (n = 2)	43.27	0.79	9.39	18.38	10.18	0.82	11.58	1.16	1.10	0.43	0.04	97.15
± 1s	1.20	0.30	0.98	0.77	0.58	0.08	0.09	0.09	0.10	0.05	0.02	1.86
C (n = 2)	42.49	0.48	10.22	19.38	9.57	0.83	11.64	1.17	1.05	0.39	0.03	97.24
± 1s	0.36	0.01	0.45	0.24	0.37	0.02	0.16	0.06	0.04	0.00	0.01	0.75
D (n = 3)	43.35	0.90	9.38	18.12	10.50	0.83	11.62	1.14	1.06	0.45	0.03	97.37
± 1s	0.26	0.18	0.20	0.58	0.31	0.05	0.18	0.03	0.03	0.09	0.00	0.78
E (n = 2)	42.91	1.25	9.66	18.02	10.23	0.79	11.50	1.18	1.18	0.35	0.05	97.09
± 1s	0.09	0.06	0.11	0.01	0.13	0.02	0.15	0.09	0.02	0.14	0.00	0.30
Average	**43.00**	**0.85**	**9.66**	**18.47**	**10.12**	**0.82**	**11.58**	**1.16**	**1.10**	**0.40**	**0.04**	**97.21**
	MA14-AB8 (Aishihik batholith)											
A (n = 3)	45.13	0.75	7.73	17.43	11.36	0.71	11.48	1.34	0.90	0.39	0.01	97.24
± 1s	0.50	0.08	0.23	0.48	0.24	0.04	0.07	0.10	0.05	0.04	0.00	0.79
B (n= 2)	44.68	0.83	8.14	16.30	10.98	0.67	10.81	1.12	0.94	0.34	0.03	94.86
± 1s	1.03	0.09	1.36	0.51	0.93	0.05	0.95	0.06	0.17	0.12	0.02	2.23
C (n= 2)	45.02	0.57	7.87	17.48	11.40	0.76	11.53	1.31	0.86	0.39	0.01	97.19
± 1s	0.93	0.47	0.43	0.10	0.24	0.01	0.34	0.19	0.20	0.13	0.01	1.24
D (n = 2)	45.48	0.83	7.63	17.18	11.45	0.85	11.57	1.22	0.91	0.38	0.01	97.50
± 1s	1.09	0.06	0.92	0.72	0.79	0.01	0.00	0.12	0.21	0.03	0.01	1.80
E (n = 3)	44.59	1.00	7.97	17.35	11.36	0.73	11.33	1.48	0.91	0.38	0.03	97.13
± 1s	0.09	0.10	0.18	0.50	0.21	0.04	0.05	0.04	0.02	0.03	0.01	0.59
F (n = 1)	45.08	0.92	7.83	17.02	11.54	0.74	11.68	1.11	0.87	0.56	0.02	97.38
± 1s	N/A	N/A	N/A	N/A	N/A	N/A	N/A	N/A	N/A	N/A	N/A	N/A
Average	**45.00**	**0.82**	**7.86**	**17.13**	**11.35**	**0.74**	**11.40**	**1.26**	**0.90**	**0.41**	**0.02**	**96.88**
	MA14-AB10 (Aishihik batholith)											
A (n = 4)	42.00	0.92	10.20	18.29	9.90	0.73	11.47	1.00	1.27	0.18	0.04	96.00
± 1s	0.73	0.11	0.49	0.70	0.26	0.04	0.17	0.08	0.04	0.07	0.01	1.18
B (n = 3)	42.11	0.92	10.35	18.72	9.72	0.74	11.62	1.05	1.22	0.15	0.03	96.63
± 1s	0.17	0.07	0.02	0.17	0.10	0.03	0.05	0.03	0.05	0.02	0.01	0.29
C (n = 3)	43.12	1.10	9.31	17.75	10.52	0.75	11.40	1.09	1.10	0.33	0.05	96.52
± 1s	1.17	0.08	0.86	0.74	0.55	0.05	0.13	0.03	0.12	0.05	0.01	1.73
D (n = 3)	42.27	0.75	10.17	18.61	10.03	0.76	11.54	1.18	1.17	0.26	0.03	96.78
± 1s	0.40	0.15	0.13	0.19	0.05	0.03	0.30	0.05	0.08	0.04	0.01	0.58
E (n = 3)	42.15	0.84	10.20	18.28	9.82	0.74	11.54	1.17	1.18	0.27	0.04	96.22
± 1s	0.22	0.10	0.51	0.44	0.35	0.01	0.19	0.01	0.16	0.16	0.02	0.85
F (n = 4)	42.40	1.21	9.78	18.27	10.06	0.72	11.39	1.16	1.23	0.23	0.08	96.53
± 1s	0.57	0.11	0.53	0.20	0.40	0.02	0.10	0.09	0.10	0.06	0.02	0.92
Average	**42.34**	**0.96**	**10.00**	**18.32**	**10.01**	**0.74**	**11.49**	**1.11**	**1.20**	**0.24**	**0.05**	**96.45**

APPENDIX A *continued.*

	MA14-TB2 (Tatchun batholith)											
A (n = 4)	39.82	0.76	13.07	18.95	8.89	0.31	10.72	2.63	1.54	0.21	0.01	96.92
± 1s	0.04	0.18	0.14	0.22	0.10	0.04	0.08	0.17	0.16	0.03	0.01	0.42
B (n = 4)	39.86	0.86	12.85	18.99	8.82	0.34	10.60	2.56	1.53	0.24	0.02	96.65
± 1s	0.42	0.24	0.54	0.12	0.27	0.03	0.13	0.15	0.17	0.08	0.01	0.83
C (n = 4)	40.11	1.05	12.61	19.03	8.84	0.31	10.46	2.56	1.41	0.17	0.02	96.56
± 1s	0.34	0.09	0.08	0.26	0.19	0.02	0.13	0.11	0.02	0.09	0.01	0.52
D (n = 4)	40.08	0.93	12.87	18.74	8.91	0.33	10.64	2.60	1.48	0.24	0.01	96.83
± 1s	0.49	0.13	0.29	0.12	0.15	0.01	0.13	0.13	0.15	0.09	0.01	0.66
E (n = 4)	40.15	1.10	12.71	18.75	8.99	0.34	10.68	2.67	1.39	0.22	0.01	97.01
± 1s	0.18	0.06	0.13	0.22	0.16	0.02	0.09	0.05	0.03	0.02	0.01	0.37
Average	**40.00**	**0.94**	**12.82**	**18.89**	**8.89**	**0.33**	**10.62**	**2.61**	**1.47**	**0.22**	**0.01**	**96.79**
	MA14-TB4 (Tatchun batholith)											
A (n = 3)	38.49	1.01	13.12	20.29	7.69	0.48	10.44	2.66	1.59	0.16	0.01	95.95
± 1σ	0.88	0.06	0.63	0.80	0.57	0.03	0.12	0.14	0.23	0.03	0.00	1.50
B (n = 3)	37.96	0.92	13.63	21.68	6.80	0.46	10.50	2.44	1.88	0.19	0.01	96.46
± 1σ	0.05	0.08	0.20	0.20	0.13	0.03	0.11	0.05	0.17	0.05	0.01	0.39
C (n = 4)	38.49	1.13	13.35	21.00	7.21	0.50	10.46	2.65	1.54	0.15	0.01	96.50
± 1σ	0.17	0.10	0.18	0.17	0.16	0.02	0.15	0.08	0.14	0.08	0.01	0.43
D (n = 3)	38.58	1.05	13.40	21.35	7.09	0.46	10.53	2.68	1.64	0.10	0.02	96.88
± 1σ	0.48	0.00	0.39	0.33	0.15	0.04	0.16	0.10	0.15	0.07	0.00	0.76
E (n = 3)	39.05	1.07	12.90	21.54	7.11	0.50	10.58	2.45	1.68	0.19	0.01	97.08
± 1σ	0.16	0.21	0.22	0.45	0.23	0.02	0.08	0.04	0.06	0.03	0.01	0.62
Average	**38.51**	**1.04**	**13.28**	**21.17**	**7.18**	**0.48**	**10.50**	**2.58**	**1.66**	**0.16**	**0.01**	**96.57**
	MA14-TB10 (Tatchun batholith)											
A (n = 4)	40.72	0.82	11.29	20.22	8.43	0.50	11.15	1.84	1.59	0.25	0.03	96.83
± 1σ	0.21	0.13	0.22	0.22	0.15	0.03	0.05	0.05	0.15	0.08	0.01	0.46
B (n = 4)	40.21	0.77	12.02	20.41	8.23	0.50	11.17	1.84	1.66	0.24	0.03	97.07
± 1σ	0.16	0.03	0.07	0.29	0.15	0.06	0.08	0.16	0.09	0.07	0.01	0.43
C (n = 4)	40.63	0.89	11.38	20.47	8.23	0.52	11.08	1.79	1.56	0.17	0.03	96.75
± 1σ	0.35	0.06	0.24	0.30	0.16	0.04	0.05	0.09	0.05	0.06	0.01	0.57
D (n = 4)	40.52	0.74	11.84	20.22	8.35	0.50	11.17	1.78	1.61	0.28	0.02	97.04
± 1σ	0.28	0.15	0.12	0.31	0.22	0.01	0.05	0.05	0.03	0.05	0.01	0.52
E (n = 4)	40.12	0.79	11.96	20.71	8.00	0.47	11.21	1.83	1.69	0.14	0.03	96.93
± 1σ	0.42	0.19	0.35	0.24	0.39	0.03	0.09	0.07	0.14	0.08	0.02	0.76
Average	**40.44**	**0.80**	**11.70**	**20.41**	**8.24**	**0.50**	**11.16**	**1.82**	**1.62**	**0.22**	**0.03**	**96.92**

Notes:
[a] FeO* denotes total Fe as FeO
[b] ±1σ errors are within-grain standard deviations in EMPA results (analytical error not included)

APPENDIX B. *Error treatment for Al-in-hornblende analyses.*

Grain	n	wt% Al	error (95%)	Al_2O_3	error (95%)	error (1σ)
MA14-AB1 (Aishihik)						
B	2	4.9	4.7	9.26	8.88	4.53
C	2	5.4	2.1	10.20	3.97	2.02
D	3	4.96	0.26	9.37	0.49	0.25
E	2	5.11	0.52	9.66	0.98	0.50
weighted average:				**9.44**	**0.43**	**0.22**
MA14-AB8 (Aishihik)						
A	3	4.09	0.31	7.73	0.59	0.30
B	2	4.3	6.4	8.12	12.09	6.17
C	2	4.2	2	7.94	3.78	1.93
D	2	4	4.4	7.56	8.31	4.24
E	3	4.22	0.24	7.97	0.45	0.23
F	1	4.1436	N/A	7.83	N/A	N/A
weighted average:				**7.88**	**0.17**	**0.09**
MA14-AB10 (Aishihik)						
A	4	5.39	0.42	10.18	0.79	0.40
B	3	5.48	0.04	10.35	0.08	0.04
C	3	4.9	1.1	9.26	2.08	1.06
D	3	5.38	0.17	10.17	0.32	0.16
E	3	5.39	0.67	10.18	1.27	0.65
F	4	5.16	0.46	9.75	0.87	0.44
weighted average:				**10.34**	**0.07**	**0.04**
MA14-TB2 (Tatchun)						
A	4	6.92	0.12	13.08	0.23	0.12
B	4	6.79	0.46	12.83	0.87	0.44
C	4	6.672	0.039	12.61	0.07	0.04
D	4	6.81	0.24	12.87	0.45	0.23
E	4	6.72	0.11	12.70	0.21	0.11
weighted average:				**12.66**	**0.19**	**0.10**
MA14-TB4 (Tatchun)						
A	3	6.94	0.82	13.11	1.55	0.79
B	3	7.21	0.26	13.62	0.49	0.25
C	4	7.06	0.16	13.34	0.30	0.15
D	3	7.09	0.51	13.40	0.96	0.49
E	3	6.83	0.29	12.91	0.55	0.28
weighted average:				**13.32**	**0.31**	**0.16**
MA14-TB10 (Tatchun)						
A	4	5.97	0.18	11.28	0.34	0.17
B	4	6.36	0.038	12.02	0.07	0.04
C	4	6.02	0.2	11.37	0.38	0.19
D	4	6.26	0.1	11.83	0.19	0.10
E	4	6.32	0.3	11.94	0.57	0.29
weighted average:				**11.95**	**0.24**	**0.12**